Hindawi
Complexity
Volume 2021, Article ID 9951162, 9 pages
https://doi.org/10.1155/2021/9951162

Research Article

Impact of Nanofluid Flow over an Elongated Moving Surface with a Uniform Hydromagnetic Field and Nonlinear Heat Reservoir

Haroon U. R. Rasheed,[1] Saeed Islam,[1] Zeeshan Khan,[2] Sayer O. Alharbi,[3] Hammad Alotaibi,[4] and Ilyas Khan[3]

[1]*Department of Mathematics, Abdul Wali Khan University Mardan, Mardan 23200, Khyber Pakhtunkhwa, Pakistan*
[2]*Sarhad University of Science and Information Technology, Peshawar 25000, Khyber Pakhtunkhwa, Pakistan*
[3]*Department of Mathematics, College of Science Al-Zulfi, Majmaah University, Al-Majmaah 11952, Saudi Arabia*
[4]*Department of Mathematics, College of Science, Taif University, P.O. Box 11099, Taif 21944, Saudi Arabia*

Correspondence should be addressed to Ilyas Khan; ilyaskhan@tdtu.edu.vn

Received 6 March 2021; Revised 9 April 2021; Accepted 29 April 2021; Published 24 May 2021

Academic Editor: Ali Akgül

The increasing global demand for energy necessitates devoted attention to the formulation and exploration of mechanisms of thermal heat exchangers to explore and save heat energy. Thus, innovative thermal transport fluids require to boost thermal conductivity and heat flow features to upsurge convection heat rate, and nanofluids have been effectively employed as standard heat transfer fluids. With such intention, herein, we formulated and developed the constitutive flow laws by utilizing the Rossland diffusion approximation and Stephen's law along with the MHD effect. The mathematical formulation is based on boundary layer theory pioneered by Prandtl. Governing nonlinear partial differential flow equations are changed to ODEs via the implementation of the similarity variables. A well-known computational algorithm BVPh2 has been utilized for the solution of the nonlinear system of ODEs. The consequence of innumerable physical parameters on flow field, thermal distribution, and solutal field, such as magnetic field, Lewis number, velocity parameter, Prandtl number, drag force, Nusselt number, and Sherwood number, is plotted via graphs. Finally, numerical consequences are compared with the homotopic solution as a limiting case, and an exceptional agreement is found.

1. Introduction

In the recent development, nanofluid has gained considerable attention from researchers, engineers, scientists, and mathematicians due to its significant implementations in diverse fields of sciences. These applications cover the following areas: chemical engineering, space science, nuclear science, solar energy collection, and several other areas. The nanofluid applications can also be employed in other real-world problems which include engine oils, heat exchangers, and thermal conductivity [1]. The word nanofluid is considered to incorporate small nanoparticles whose dimension is up to 1–100 nm in the base liquid; biofluid, lubricants, oil, and ethylene are the common examples of nanofluids [2]. Eastman et al. [3] studied to develop the thermal behavior of nanofluids by incorporating various nanosized material particles to base fluids. Chamkha et al. [4] examined radiation effects on mixed convection in view of the vertical cone embedded in the porous medium with the nanoliquid. The influence of hydromagnetic free convective and heat transfer was analyzed by Sheikholeslami et al. [5]. The consequences of MHD flow and viscous dissipation on the momentum boundary layer of the nanoliquid were evaluated by Abbas and Sayed [6]. The hydromagnetic flow of nanofluids over a revolving disk was reported by Mahanthesh et al. [7]. Later on, various potential investigations have been carried out by many researchers and engineers into the development and implications of these fluids [8–11]. Heat transfer rheology in convective flow nanofluids with thermal conductivity and electrical behavior received exceptional importance for their fruitful applications in life sciences and engineering development. Such applications include solar energy, nuclear reactor, and cooling and heating mechanisms. Using Buongiorno's model, Shehzad et al. [12] examined the effect of convective heat flow of the nanoliquid. Shen et al. [13] investigated the heat flow of a nanoliquid by a stretching surface with thermal radiation effect and velocity slip. Jahan et al. [14] evaluated the numerical solution to understand heat transfer aspects in nanomaterials over a convectively permeable stretching surface with radiation effect. Hamad and Pop [15] described thermal radiation effects on unsteady nanoliquid over an oscillatory moving plate with the heat reservoir. Sheikholeslami and Ganji [16] conducted a numerical consequence to analyze the three-dimensional nanoliquid with thermal radiation effects in a revolving system. Hussain et al. [17] illustrated analytical results by employing Laplace transform to explore unsteady hydromagnetic flow over a rotating system subject to chemical reaction and Hall current. Several mathematicians and investigators reported the thermal conductivity and electrical conductivity nature of nanofluids under different conditions with various geometry convective heat transfer effects in [18–23]. Mahanthesh et al. [24] evaluated the impact of suspended nanoparticles on the convective flow of nanomaterial in view of the vertical surface with radiation effects. Kumar et al. [25] conducted a numerical study by employing the RK-4 method to analyze radiative Jeffrey nanofluid flow with convective boundary conditions. Raza et al. [26] numerically studied the influence of viscous dissipation and magnetic field of molybdenum disulfide nanoliquid with the shape effect. Al-Odat et al. [27] addressed the interaction of magnetic effects and boundary layer flow of the fluid by an exponentially stretchable sheet. Chamkha and Aly [28] presented the numerical solution to magnetohydrodynamic free convection flow of a nanoliquid by a vertical plane in view of the porous medium and radiation effects. Aliakbar et al. [29] studied the analytical solution to hydromagnetic flow of upper convective Maxwell fluid past a stretchable extended surface. Khan et al. [30] evaluated the numerical solution by utilizing the explicit finite difference method (FDM) with stability analysis to unsteady nanofluid flow by a stretching surface. Ibrahim and Shankar [31] employed the shooting technique to inspect magnetohydrodynamic boundary layer flow of nanomaterial over the stretching sheet with the slip condition. Sparrow and Cess [32], Ozisik [33], Siegel and Howell [34], Howell [35], Takhar et al. [36], and Hossain and Takhar [37] all contributed well to radiative heat transfer analysis.

2. Basic Flow Equations

Here, we considered steady magnetohydrodynamic boundary layer nanofluid flow with a uniform velocity U moving towards an infinite plate. The velocity of the infinite plate is defined by the relation $U_w = \lambda U$; here, λ denotes the velocity parameter. The nanofluid flow is confined at $0 \le y$. The coordinate system is chosen in the form such that the $y-$axis is normal to the direction of flow, and the magnetic interaction is employed normal to the plate. Let T_w be the fluid temperature and C_w be the concentration at the wall, and free-stream numbers are T_∞ and C_∞. The proposed model is described by the following set of differential equations. The flow map and coordinates axes are presented in Figure 1.

$$\frac{\partial u}{\partial x} + \frac{\partial v}{\partial y} = 0, \tag{1}$$

$$u\frac{\partial u}{\partial x} + v\frac{\partial u}{\partial y} = v\frac{\partial^2 v}{\partial y^2} - u\frac{\sigma B_0^2}{\rho_f}, \tag{2}$$

$$u\frac{\partial T}{\partial x} + v\frac{\partial T}{\partial y} = \alpha\frac{\partial^2 T}{\partial y^2} - \frac{\alpha}{k}\frac{\partial q_r}{\partial y} + \tau\left(D_B\frac{\partial C}{\partial y}\frac{\partial T}{\partial y} + \frac{D_T}{T_\infty}\left(\frac{\partial T}{\partial y}\right)^2\right), \tag{3}$$

$$u\frac{\partial u}{\partial x} + v\frac{\partial u}{\partial y} = D_B\left(\frac{\partial^2 C}{\partial y^2}\right) + \frac{D_T}{T_\infty}\left(\frac{\partial^2 T}{\partial y^2}\right). \tag{4}$$

Here, (u, v) are the velocity components in coordinates axes, v is the kinematic viscosity, k is the thermal conductivity parameter, q_r denotes the heat flux, D_B represents Brownian diffusion coefficient, D_T represents the thermophoresis diffusion coefficient, B_0 denotes the field strength, σ is the electrical conductivity parameter, τ represents the ratio of the nanoparticle heat capacity to the base fluid heat capacity, τ_w is the shear stress, $\alpha = k/(\rho c)_f$ represents thermal diffusivity, λ is the velocity parameter, $\lambda > 0$ corresponds to the downstream motion of the plate from the origin, and $\lambda < 0$ corresponds to the upstream motion.

The appropriate extreme values are

$$\begin{aligned} &y = 0\colon\ v = 0, u = \lambda U, T = T_w, C = C_w, \\ &y \longrightarrow \infty\colon\ U_w \longrightarrow U, T \longrightarrow T_\infty, C \longrightarrow C_\infty. \end{aligned} \tag{5}$$

Utilizing the Rosseland diffusion approximation [35], thermal flux is defined as

$$q_r = \frac{-4\sigma^*}{3K_s}\frac{\partial T^4}{\partial y}, \tag{6}$$

where σ^* is the Stefan–Boltzman constant and K_S is the Rosseland mean absorption coefficient. The difference in the nanofluid temperature within the fluid is sufficiently small such that T^4 can be written as a linear function of temperature:

$$T^4 \cong 4TT_\infty^3 - 3T_\infty^4. \tag{7}$$

Substituting (6) and (7) in (3), we attained

$$\frac{\partial q_r}{\partial y} = \frac{-16\sigma^* T_\infty^3}{3K_s}\frac{\partial^2 T}{\partial y^2}. \tag{8}$$

Introduce the similarity transformations:

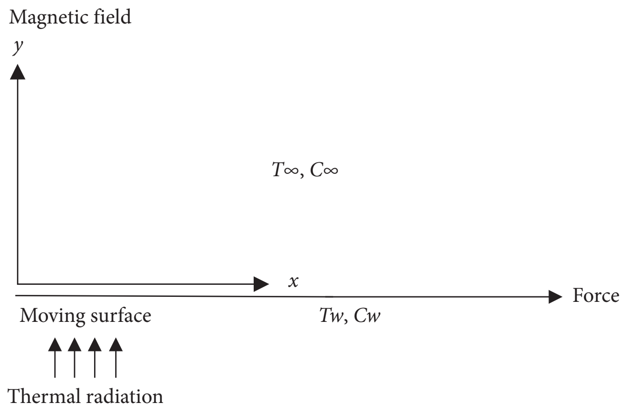

Figure 1: The flow map diagram.

$$\begin{aligned}\psi &= (2U\nu x)^{(1/2)} f(\eta),\\ \theta(\eta) &= \frac{T-T_\infty}{T_w-T_\infty},\\ \varphi(\eta) &= \frac{C-C_\infty}{C_w-C_\infty},\\ \eta &= (U/2\nu x)^{(1/2)}.\end{aligned} \tag{9}$$

The stream function ψ may be expressed as

$$\begin{aligned}u &= \frac{\partial\psi}{\partial y},\\ v &= -\frac{\partial\psi}{\partial x}.\end{aligned} \tag{10}$$

Equation (1) is justified automatically, while equations (2)–(5) have the forms

$$f'''(\eta) + f(\eta)f''(\eta) - (\mathrm{Ha})f'(\eta) = 0, \tag{11}$$

$$\frac{1}{\mathrm{pr}}(3+4R)\theta''(\eta) + f(\eta)\theta'(\eta) + \mathrm{Nb}\varphi'(\eta)\theta'(\eta) + \mathrm{Nt}\left(\theta'(\eta)\right)^2 = 0, \tag{12}$$

$$\varphi''(\eta) + (\mathrm{Le})f(\eta)\varphi'(\eta) + \left(\frac{\mathrm{Nt}}{\mathrm{Nb}}\right)\theta''(\eta) = 0, \tag{13}$$

$$\begin{aligned}f(0) &= 0,\\ f'(0) &= \lambda,\\ \theta(0) &= 1,\\ \varphi(0) &= 1,\\ f'(\infty) &\longrightarrow 1,\\ \theta(\infty) &\longrightarrow 0,\\ \varphi(\infty) &\longrightarrow 0.\end{aligned} \tag{14}$$

The governing variables appearing in (11)–(13) are defined as follows. $R = (4\alpha\delta T_\infty^3/kk)$, $\mathrm{Pr} = (\nu/\alpha)$, $\mathrm{Le} = (\nu/D_B)$, $\mathrm{Ha} = (2xB_0^2/U\rho_f)$, $\mathrm{Nb} = (((\rho c)_p D_B(\varphi_w - \varphi_\infty))/\nu(\rho c)_f)$, $\mathrm{Nt} = (((\rho c)_p D_B(T_w - T_\infty))/\nu(\rho c)_f T_\infty)$, $C_f = (\tau_w/\rho u^2)$, $\mathrm{Nu}_x = (q_w/(T_w - T_\infty)k)$, and $\mathrm{Sh}_x = (xq_m/D_B(C_w - C_\infty)k)$ label the radiation constraint, Prandtl number, Lewis number, Hartmann number, Brownian parameter, thermophoretic force, drag force, and Nusselt and Sherwood numbers.

The local Reynolds number is given by the equation $\mathrm{Re}_x = Ux/\nu$.

Using similarity variables in C_f, Nu_x, and Sh_x, we get the dimensionless form as

$$\begin{aligned}(2\mathrm{Re})^{0.5}C_f &= f''(0),\\ \left(\frac{\mathrm{Re}_x}{2}\right)^{-1}2\mathrm{Nu}_x &= -\theta'(0),\\ \left(\frac{\mathrm{Re}_x}{2}\right)^{-1}2\mathrm{Nu}_x &= -\varphi'(0).\end{aligned} \tag{15}$$

3. Numerical Solution and Convergence Analysis

The nonlinear flow expressions (ODEs) in (11)–(13) subject to boundary conditions in (14) are first transformed into 1^{st}-order ODEs and then tackled numerically by employing a built-in computational algorithm BVPh2 in Mathematica software. The routine flow numerical code is demonstrated in Figure 2. Step size $\Delta\eta = 0.001$, and relative tolerance error 10^{-6} is set; in addition, the choice of $\eta_\infty = 7$ confirms that all numerical approximations approach correctly to asymptotic values.

Let us introduce the transformation variables as $f(\eta) = w_1, f'(\eta) = w_2, f''(\eta) = w_3, \theta(\eta) = w_4, \theta'(\eta) = w_5, \quad \phi(\eta) = w_6$, and $\phi'(\eta) = w_7$; hence, the following system of 1^{st}-order seven differential equations are generated:

$$\begin{aligned}w_1' &= w_2,\\ w_2' &= w_3,\\ w_3' + w_1w_3 - (\mathrm{Ha})w_2 &= 0,\\ w_4' &= w_5,\\ \frac{1}{\mathrm{pr}}(3+4R)w_5' + w_1w_5 + (\mathrm{Nb})w_5w_7 + \mathrm{Nt}\left(w_5\right)^2 &= 0,\\ w_6' &= w_7,\\ w_7' + (\mathrm{Le})w_1w_7 + \left(\frac{\mathrm{Nt}}{\mathrm{Nb}}\right)w_5 &= 0.\end{aligned} \tag{16}$$

The transfer conditions are

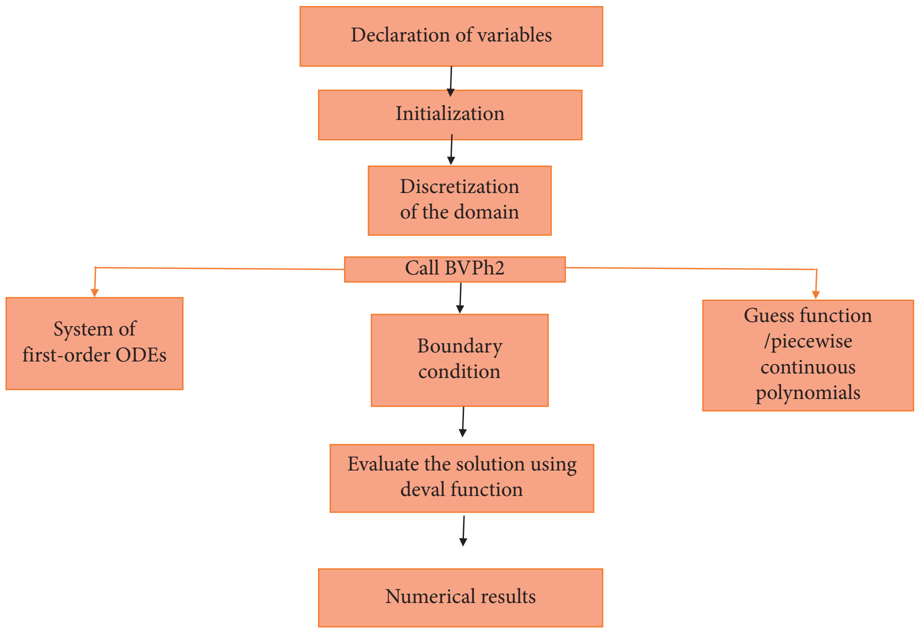

Figure 2: BVPh2 routine algorithm in Mathematica software.

$$
\begin{aligned}
w_1(0) &= 0, \\
w_2(0) &= \lambda, \\
w_4(0) &= 1, \\
w_6(0) &= 1, \\
w_2(\infty) &= 1, \\
x_4(\infty) &= 0, \\
x_6(\infty) &= 0.
\end{aligned}
\tag{17}
$$

For authentication purpose, the computational results are further tested by the use of an analytical scheme (HAM), and a reasonable agreement has been obtained in two solutions. The attributes of two solutions via graphs are shown in Figures 3–5, and the tabulized data for velocity and thermal and solutal fields are presented in Tables 1–3. Finally, the residual error analysis has been evaluated and shown in Figure 6. A decrease in error is perceived for higher-order deformations.

4. Discussion

The current computational results accomplished by a numerical algorithm BVP2 unveil the influence of pertinent governing constraints on velocity, thermal field, and concentration profile. The impact of various emerging parameters in flow equations (11)–(13) is plotted through Figures 7–19. The numerical values of these flow factors are regarded as $\mathrm{Ha} = 0.5, \lambda = 0.3, \mathrm{Nt} = 0.5, \mathrm{Nb} = 0.5$, $\mathrm{Le} = 1.0$, $\mathrm{Pr} = 2.0$, and $R = 0.4$.

Figure 7 describes the Hartmann number Ha effect on the nanofluid velocity profile $f'(\eta)$. As anticipated, $f'(\eta)$ dwindles when subject to upsurge in Ha. In reality, this figure revealed that augmentation in Ha boosts Lorentz force. In consequence, velocity $f'(\eta)$ diminishes. The

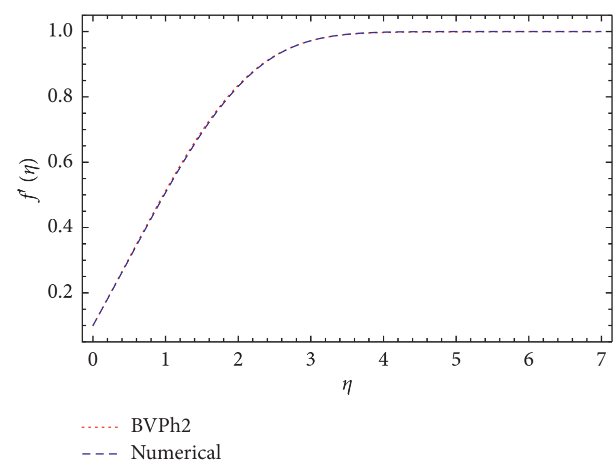

Figure 3: Graphical comparison for two solutions in case of the velocity profile.

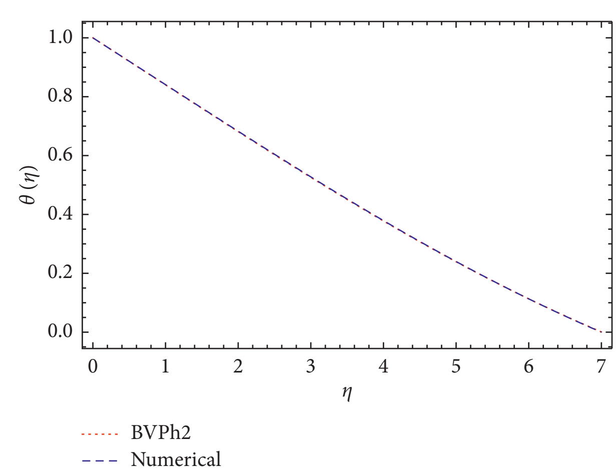

Figure 4: Graphical comparison for two solutions in case of the temperature profile.

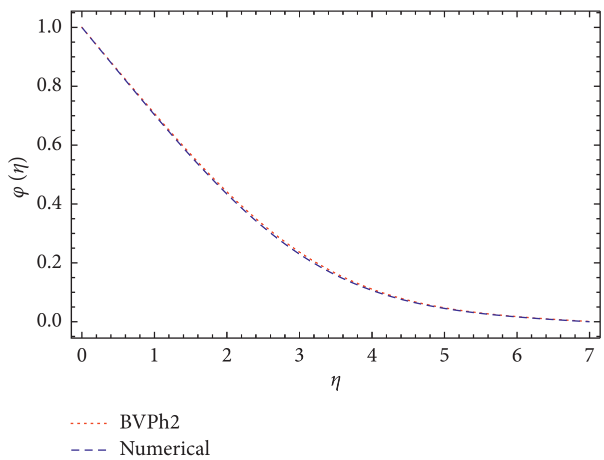

Figure 5: Graphical comparison for two solutions in case of the concentration profile.

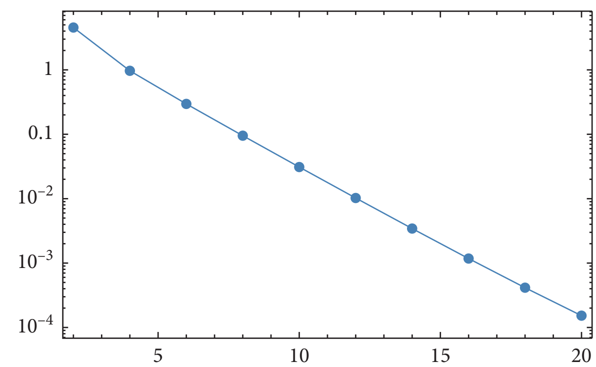

Figure 6: Total residual error via the order of approximation.

Table 1: Numerical solution via the analytical solution for the velocity $f'(\eta)$ profile.

η	Numerical solution	HAM solution	Absolute error
0.0	0.000000	1.260600×10^{-11}	1.260600×10^{-11}
1.0	0.304039	0.306972	0.002933
2.0	0.987469	0.995322	0.007853
3.0	1.904260	1.913580	0.009316
4.0	2.893680	2.902320	0.008634
5.0	3.893100	3.900560	0.007458
6.0	4.893080	4.899550	0.006471
7.0	5.893080	5.898930	0.005845

Table 2: Numerical solution via the analytical solution for the temperature $\theta(\eta)$ profile.

η	Numerical solution	HAM solution	Absolute error
0.0	1.000000	1.000000	7.586150×10^{-13}
1.0	0.840974	0.840241	0.000733
2.0	0.682654	0.681360	0.001294
3.0	0.527582	0.526044	0.001539
4.0	0.379004	0.377623	0.001381
5.0	0.240021	0.239184	0.000837
6.0	0.113119	0.113103	0.000016
7.0	7.995770×10^{-10}	0.000912	0.000912

Table 3: Numerical solution via the analytical solution for the nanoparticle concentration $\varphi(\eta)$ profile.

η	Numerical solution	HAM solution	Absolute error
0.0	1.000000	1.000000	2.065240×10^{-12}
1.0	0.703260	0.707816	0.004557
2.0	0.433740	0.441075	0.007335
3.0	0.229562	0.236590	0.007028
4.0	0.106379	0.110674	0.004295
5.0	0.045187	0.047072	0.001885
6.0	0.016303	0.017325	.001021
7.0	$-2.066080'' \times 10^{-8}$	0.000912	0.000912

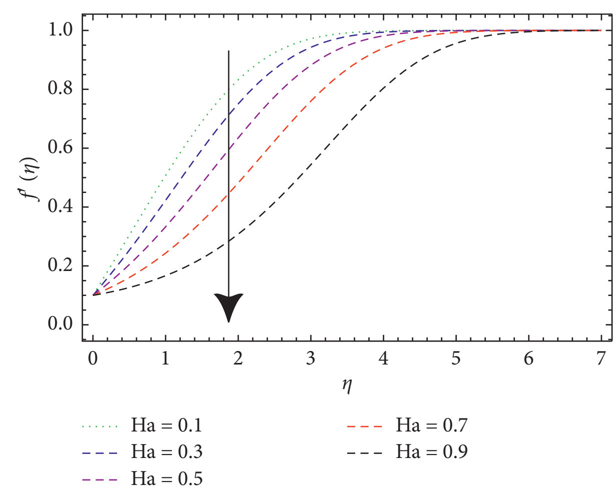

Figure 7: Influence of the velocity $f'(\eta)$ profile via Ha.

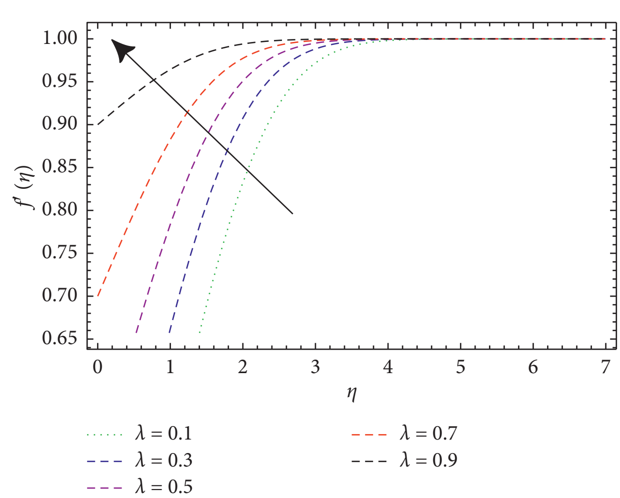

Figure 8: Influence of the velocity $f'(\eta)$ profile via λ.

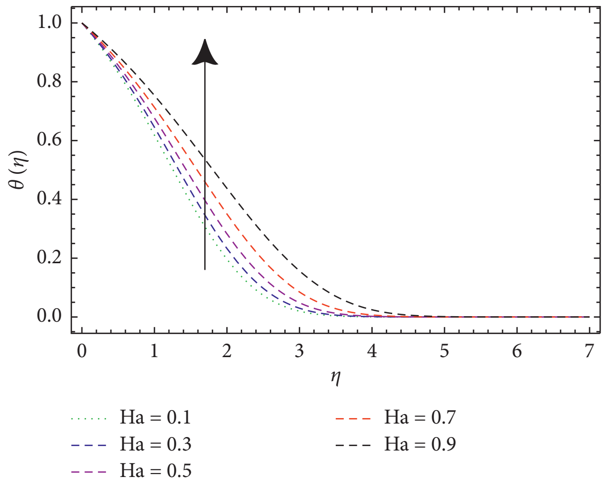

FIGURE 9: Influence of the temperature $\theta(\eta)$ profile via Ha.

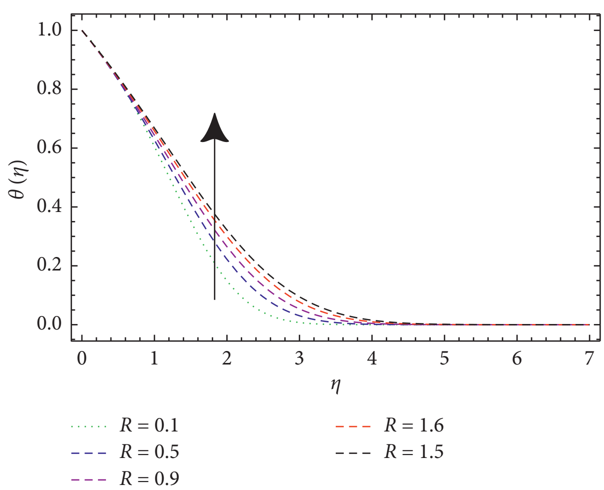

FIGURE 10: Influence of the temperature $\theta(\eta)$ profile via R.

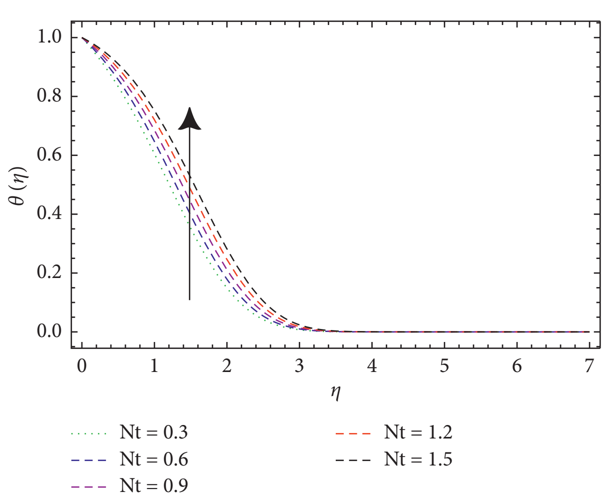

FIGURE 11: Influence of the temperature $\theta(\eta)$ profile via Nt.

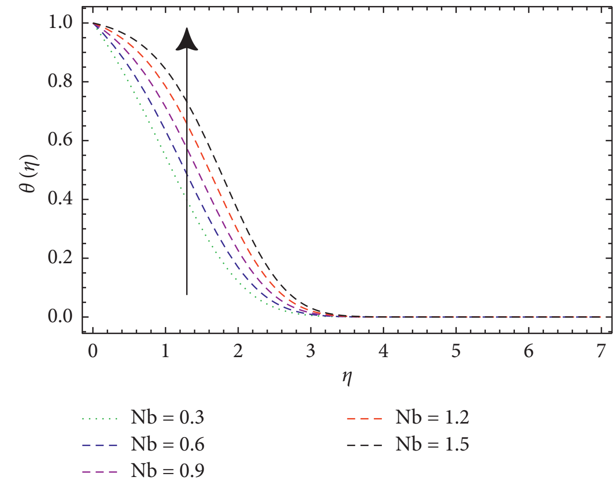

FIGURE 12: Influence of the $\theta(\eta)$ profile via Nb.

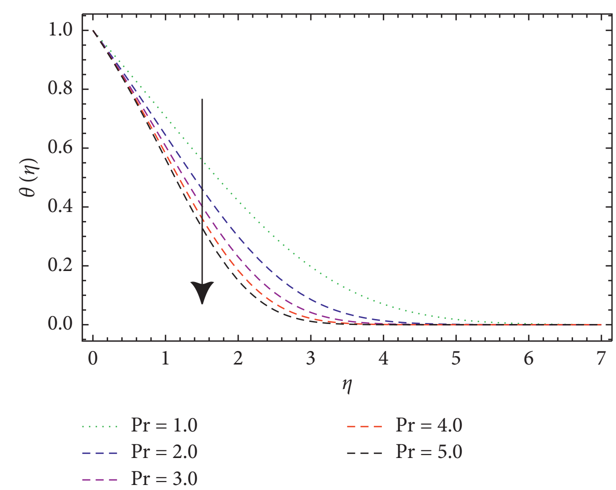

FIGURE 13: Influence of the $\theta(\eta)$ profile via Pr.

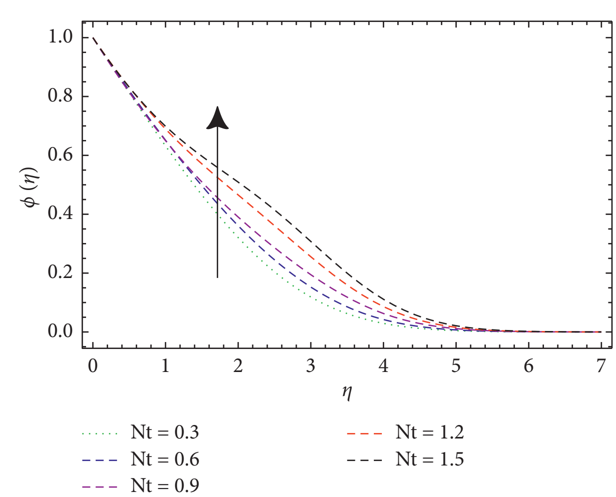

FIGURE 14: Influence of the temperature $\phi(\eta)$ profile via Nt.

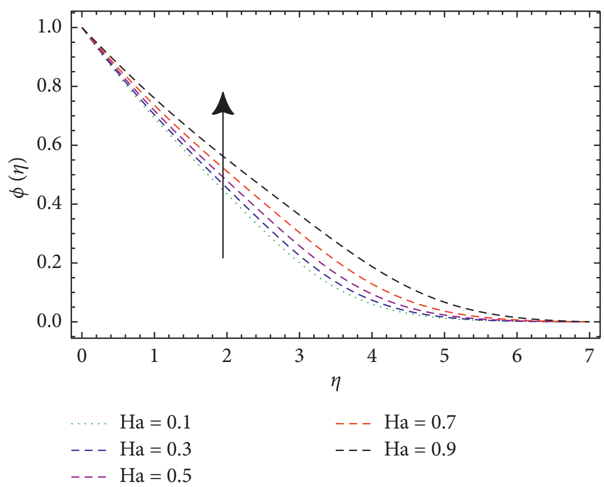

FIGURE 15: Influence of the $\phi(\eta)$ profile via Ha.

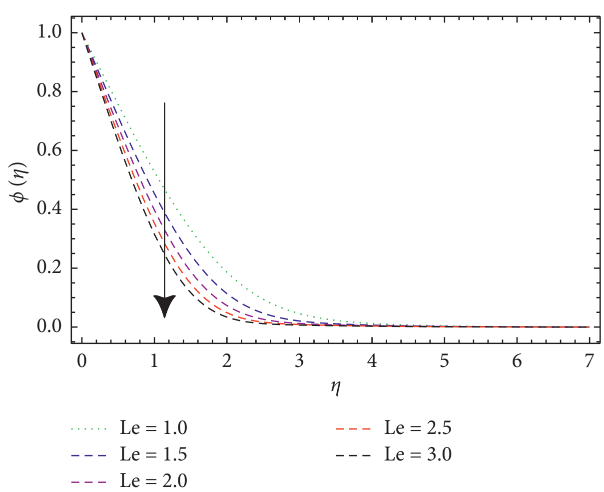

FIGURE 16: Influence of the $\phi(\eta)$ profile via Le.

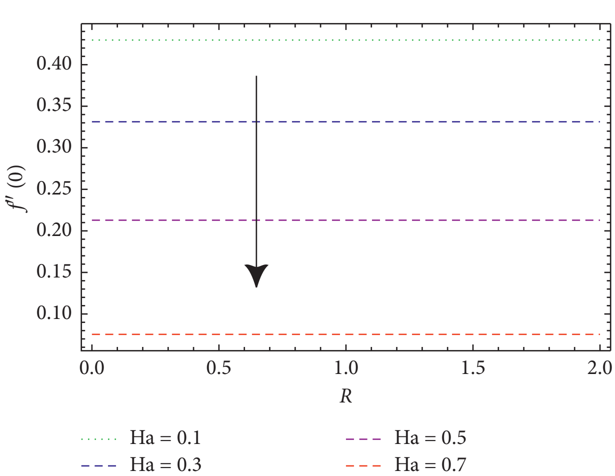

FIGURE 17: Skin friction/drag force via R for different values of Ha.

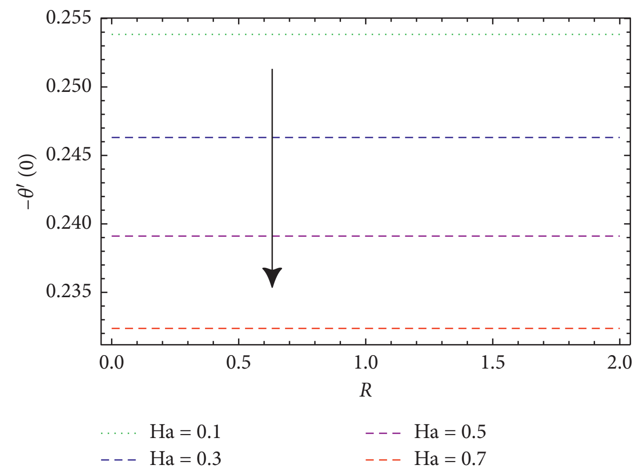

FIGURE 18: Nusselt number via R for different values of Ha.

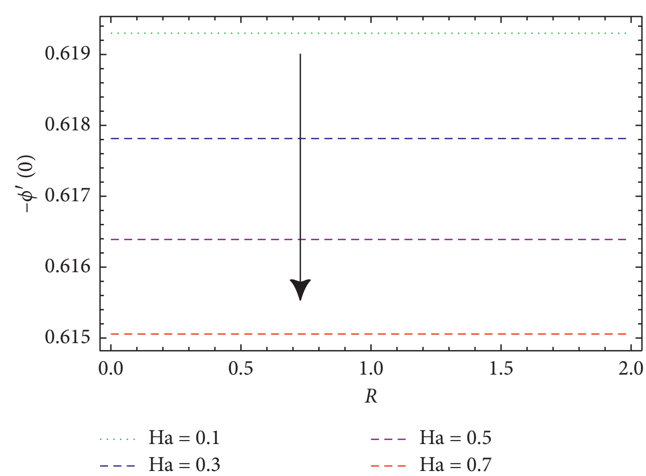

FIGURE 19: Sherwood number via R for changed values of Ha.

contribution of velocity parameter λ on nanofluid velocity profile $f'(\eta)$ is evaluated through Figure 8. As perceived, in this figure, fluid velocity enhances when λ upsurges. Hence, $f'(\eta)$ upsurges. The attributes of thermal field $\theta(\eta)$ curves for Ha magnetic field are disclosed in Figure 9. One can perceive that $\theta(\eta)$ is a growing function of Ha. In reality, the heat transfer rate of nanofluid particles boosts up through larger Ha. Consequently, $\theta(\eta)$ escalates. Such a scenario is perceived because higher Ha implies larger Lorentz force provides more resistance which makes increases the fluid flow. In consequence, $\theta(\eta)$ augments. Figure 10 explains variations in thermal field $\theta(\eta)$ subjected to radiation parameter R. This figure unveils $\theta(\eta)$ enhancement for higher values of (R). In fact, working nanofluid acquires extra heat subject to the radiation factor. In consequence, $\theta(\eta)$ upsurges. ;Figure 11 reveals variations in $\theta(\eta)$ subject to thermophoresis parameter Nt. Here, thermal field increases with increasing Nt. Physically, the thermophoretic force rises as Nt parameter is escalated. Such force is responsible to move small size particles by hotter towards colder region. Consequently, $\theta(\eta)$ escalates. Figure 12 explains the Brownian motion parameter Nb effect on $\theta(\eta)$. As anticipated, thermal field $\theta(\eta)$ enhances through larger Nb parameter. In nanofluids, Brownian motion ascends due to small-size nanoparticles, and at this point, nanoparticle motion rate and its effect against the fluid have a vital vibrant role regarding heat transport. In consequence, upsurges in Nb produce active nanoparticle motion within the base fluid. The result of disordered nanoparticle motion develops kinetic energy of the nanoparticles, and eventually, thermal behavior $\theta(\eta)$ of the fluid augments. The contribution of Prandtl number Pr on $\theta(\eta)$ is evaluated through Figure 13. Here, thermal field diminishes against larger Prandtl number estimations. Attributes of Nt on solutal field $\varphi(\eta)$ are interpreted in Figure 14. We perceived an increase in $\varphi(\eta)$ subjected to higher thermophoresis parameter estimations. In reality, an upsurge in thermophoresis force is viewed through greater Nt parameter which is responsible for moving the fluid particles from higher temperature to lower temperature. In consequence, $\varphi(\eta)$ profile boosts. Solutal field $\varphi(\eta)$ curves for Hartmann number Ha are unveiled in Figure 15. Clearly, the solutal field is the augmenting function of the Hartmann number. Mass transfer augments when Ha is enhanced. Accordingly, $\varphi(\eta)$ increases. The attributes of Lewis number parameter Le on solutal field $\varphi(\eta)$ are interpreted in Figure 16. Clearly, $\varphi(\eta)$ diminishes when Le is increased. Physically, Lewis number Le signifies the influence of thermal diffusion on mass diffusion in the boundary layer region. Such a scenario is noticed because higher Le implies lessening in the solutal field and boundary layer.

Effects of pertinent variables against physical quantities $(f''(0), -\theta'(0), \text{and } -\varphi'(0))$ are described in Figures 17–19. These figures highlight decay in $f''(0)$, $-\theta'(0)$, and $-\varphi'(0)$ for larger R and Ha estimations.

5. Closing Remarks

The aim of this research is to analyze two-dimensional incompressible viscoelastic magnetonanofluid flow with the Buongiorno model. This investigation further includes results of heat generation/absorption with convective conditions. Current investigation enables us to explain the following key outcomes:

(i) Velocity field $f'(\eta)$ lessens when subject to increment in the Hartmann number Ha, and thermal field $\theta(\eta)$ develops with magnetic strength

(ii) Velocity profile augmented with larger velocity parameter λ

(iii) Thermal field $\theta(\eta)$ upsurges when radiation parameter R and Hartmann number Ha are improved

(iv) A similar feature is viewed qualitatively for higher thermophoretic parameter Nt and Brownian motion variable Nb

(v) Solutal field $\varphi(\eta)$ boosts through larger Hartmann number Ha, and $\varphi(\eta)$ field dwindles while Lewis number Le augments

(vi) Larger values of radiation parameter R and Hartmann number Ha diminish $f''(0)$ skin friction (drag force), Nusselt number $-\theta'(0)$, and Sherwood number $-\varphi'(0)$

Data Availability

The data used to support the findings of this study are included within the article.

Conflicts of Interest

The authors declare that they have no conflicts of interest.

Acknowledgments

The authors extend their appreciation to the Deanship of Scientific Research at Majmaah University for funding this work under the project number (RGP-2019-6).

References

[1] T. Hayat, R. Sajjad, A. Alsaedi, T. Muhammad, and R. Ellahi, "On squeezed flow of couple stress nanofluid between two parallel plates," *Results in Physics*, vol. 7, pp. 553–561, 2017.

[2] S. U. S. Choi and J. A. Eastman, "Enhancing thermal conductivity of fluids with nanoparticles," in *Proceedings of the ASME International Mechanical Engineering Congress and Exposition*, pp. 99–105, San Francisco, CA, USA, January 1995.

[3] J. A. Eastman, S. U. S. Choi, S. Li, W. Yu, and L. J. Thompson, "Anomalously increased effective thermal conductivities of ethylene glycol-based nanofluids containing copper nanoparticles," *Applied Physics Letters*, vol. 78, pp. 718–720, 2001.

[4] A. J. Chamkha, S. Abbasbandy, A. M. Rashad, and K. Vajravelu, "Radiation effects on mixed convection about a cone embedded in a porous medium filled with a nanofluid," *Meccanica*, vol. 48, pp. 275–285, 2013.

[5] M. Sheikholeslami, M. M. Rashidi, T. Hayat, and D. D. Ganji, "Free convection of magnetic nanofluid considering MFD viscosity effect," *Journal of Molecular Liquids*, vol. 218, pp. 393–399, 2016.

[6] W. Abbas and E. A. Sayed, "Hall current and joule heating effects on free convection flow of a nanofluid over a vertical cone in presence of thermal radiation," *Thermal Science*, vol. 21, pp. 2603–2614, 2017.

[7] B. Mahanthesh, B. Gireesha, I. Animasaun, T. Muhammad, and N. Shashikumar, "MHD flow of SWCNT and MWCNT nanoliquids past a rotating stretchable disk with thermal and exponential space dependent heat source," *Physica Scripta*, vol. 94, Article ID 085214, 2019.

[8] I. L. Animasaun, O. K. Koriko, K. S. Adegbie et al., "Comparative analysis between 36 nm and 47 nm alumina-water nanofluid flows in the presence of Hall effect," *Journal of Thermal Analysis and Calorimetry*, vol. 135, pp. 873–886, 2019.

[9] I. Ullah, S. Shafie, I. Khan, and K. L. Hsiao, "Brownian diffusion and thermophoresis mechanisms in Casson fluid over a moving wedge," *Results in Physics*, vol. 9, pp. 183–194, 2018.

[10] P. B. S. Kumar, B. J. Gireesha, R. S. R. Gorla, and B. Mahanthesh, "Magnetohydrodynamic flow of Williamson nanofluid due to an exponentially stretching surface in the

presence of thermal radiation and chemical reaction," *Journal of Nanofluids*, vol. 6, pp. 264–272, 2017.

[11] X. Zhou, Y. Jiang, X. Li et al., "Numerical investigation of heat transfer enhancement and entropy generation of natural convection in a cavity containing nano liquid-metal fluid," *International Communications in Heat and Mass Transfer*, vol. 106, pp. 46–54, 2019.

[12] N. Shehzad, A. Zeeshan, R. Ellahi, and K. Vafai, "Convective heat transfer of nanofluid in a wavy channel: Buongiorno's mathematical model," *Journal of Molecular Liquids*, vol. 222, pp. 446–455, 2016.

[13] B. Shen, L. Zheng, C. Zhang, and X. Zhang, "Bioconvection heat transfer of a nanofluid over a stretching sheet with velocity slip and temperature jump," *Thermal Science*, vol. 21, pp. 2347–2356, 2017.

[14] S. Jahan, H. Sakidin, R. Nazar, and I. Pop, "Analysis of heat transfer in nanofluid past a convectively heated permeable stretching/shrinking sheet with regression and stability analyses," *Results in Physics*, vol. 10, pp. 395–405, 2018.

[15] M. A. A. Hamad and I. Pop, "Unsteady MHD free convection flow past a vertical permeable flat plate in a rotating frame of reference with constant heat source in a nanofluid," *Heat and Mass Transfer*, vol. 47, pp. 1517–1524, 2011.

[16] M. Sheikholeslami and D. D. Ganji, "Three-dimensional heat and mass transfer in a rotating system using nanofluid," *Powder Technology*, vol. 253, pp. 789–796, 2014.

[17] S. M. Hussain, J. Jain, G. S. Seth, and M. M. Rashidi, "Free convective heat transfer with Hall effects, heat absorption and chemical reaction over an accelerated moving plate in a rotating system," *Journal of Magnetism and Magnetic Materials*, vol. 422, pp. 112–123, 2017.

[18] X. Zhou, Y. Jiang, Y. Hou, and M. Du, "Thermocapillary convection instability in annular two-layer system under various gravity levels," *Microgravity Science and Technology*, vol. 31, pp. 641–648, 2019.

[19] Y. Jiang and X. Zhou, "Heat transfer and entropy generation analysis of nanofluids thermocapillary convection around a bubble in a cavity," *International Communications in Heat and Mass Transfer*, vol. 105, pp. 37–45, 2019.

[20] Y. Jiang, X. Zhou, and Y. Wang, "Effects of nanoparticle shapes on heat and mass transfer of nanofluid thermocapillary convection around a gas bubble," *Microgravity Science and Technology*, vol. 32, pp. 1–11, 2019.

[21] Y. Jiang, X. Zhou, and Y. Wang, "Comprehensive heat transfer performance analysis of nanofluid mixed forced and thermocapillary convection around a gas bubble in minichannel," *International Communications in Heat and Mass Transfer*, vol. 110, Article ID 104386, 2020.

[22] B. Mahanthesh, B. J. Gireesha, R. S. R. Gorla, F. M. Abbasi, and
S. A. Shehzad, "Numerical solutions for magnetohydrodynamic flow of nanofluid over a bidirectional non-linear stretching surface with prescribed surface heat flux boundary," *Journal of Magnetism and Magnetic Materials*, vol. 417, pp. 189–196, 2016.

[23] N. Bhaskar Reddy, T. Poornima, and P. Sreenivasulu, "Influence of variable thermal conductivity on MHD boundary layer slip flow of ethylene-glycol based cu nanofluids over a stretching sheet with convective boundary condition," *International Journal of Engineering Mathematics*, vol. 2014, Article ID 905158, 10 pages, 2014.

[24] B. Mahanthesh, J. Gireesha, and I. L. Animasaun, "Exploration of non-linear thermal radiation and suspended nanoparticles effects on mixed convection boundary layer flow of nano-liquids on a melting vertical surface," *Journal of Nanofluids*, vol. 7, pp. 833–843, 2018.

[25] P. S. Kumar, B. Mahanthesh, B. Gireesha, and S. Shehzad, "Quadratic convective flow of radiated nano-Jeffrey liquid subject to multiple convective conditions and Cattaneo Christov double diffusion," *Applied Mathematics and Mechanics*, vol. 39, pp. 1311–1326, 2018.

[26] J. Raza, F. Mebarek-Oudina, and A. Chamkha, "Magnetohydrodynamic flow of molybdenum disulfide nanofluid in a channel with shape effects," *Multidiscipline Modeling in Materials and Structures*, vol. 15, pp. 737–757, 2019.

[27] M. Q. Al-Odat, R. A. Damesh, and T. A. Al-Azab, "Thermal boundary layer on an exponentially stretching continuous surface in the presence of magnetic field effect," *International Journal of Applied Mechanics and Engineering*, vol. 11, pp. 289–299, 2006.

[28] A. J. Chamkha and A. M. Aly, "MHD free convection flow of a nanofluid past a vertical plate in the presence of heat generation or absorption effects," *Chemical Engineering Communications*, vol. 198, pp. 425–441, 2011.

[29] V. Aliakbar, A. Alizadeh-Pahlavan, and K. Sadeghy, "The influence of thermal radiation on MHD flow of Maxwellian fluids above stretching sheets," *Communications in Nonlinear Science and Numerical Simulation*, vol. 14, no. 3, pp. 779–794, 2009.

[30] M. S. Khan, M. M. Alam, and M. Ferdows, "Effects of magnetic field on radiative flow of a nanofluid past a stretching sheet," *Procedia Engineering*, vol. 56, pp. 316–322, 2013.

[31] W. Ibrahim and B. Shankar, "MHD boundary layer flow and heat transfer of a nanofluid past a permeable stretching sheet with velocity, thermal and solutal slip boundary conditions," *Computers & Fluids*, vol. 75, pp. 1–10, 2013.

[32] M. E. Sparrow and D. R. Cess, *Radiation Heat Transfer*, Brooks/Cole, Belmont, CA, USA, 1970.

[33] N. M. Ozisik, *Radiative Transfer and Interaction with Conduction and Convection*, John Wiley & Sons, New York, NY, USA, 1973.

[34] R. Siegel and J. R. Howell, *Thermal Radiation Heat Transfer*, Hemisphere, New York, NY, USA, 2nd edition, 1992.

[35] J. Howell, "Radiative transfer in porous media," in *Handbook of Porous Media*, K. Vafai, Ed., CRC Press, New York, NY, USA, 2000.

[36] H. S. Takhar, R. S. R. Gorla, and V. M. Soundalgekar, "Radiation effects on MHD free convection flow of a gas past a semi-infinite vertical plate," *International Journal of Numerical Methods For Heat And Fluid Flow*, vol. 6, pp. 77–83, 1996.

[37] M. A. Hossain and H. S. Takhar, "Radiation effect on mixed convection along a vertical plate with uniform surface temperature," *Heat and Mass Transfer*, vol. 31, pp. 243–248, 1996.